Shyh-Haur Su
Graduate Student

Ching-Huan Tseng
Professor
e-mail: chtseng@cc.nctu.edu.tw

Department of Mechanical Engineering
National Chiao Tung University
Hsinchu, Taiwan 30050, R.O.C.

Synthesis and Optimization for Rotor Profiles in Twin Rotor Screw Compressors

This paper proposes a systematic synthesis method for twin-screw rotor profiles for compressors. Both ''original generating curves'' and ''generated curves'' are distributed on each rotor profile, and all the geometric parameters of these curves can be determined with satisfying the conditions of continuity in tangency by given only several specific parameter values. The contact lines on rotor surfaces and the blowhole area calculation are also presented. Three cases of optimization problems are shown in this paper and both contact-line length and blowhole area are reduced when letting the contact-line length be the object function with a constraint of blowhole area.
[S1050-0472(00)01103-X]

1 Introduction

The helical screw compressor is a positive-displacement machine; it consists of two rotors enclosed in a pressure-containing casing. The rotors differ in shape and are identified as male and female. As the rotors rotate, gas is drawn through the suction nozzle into the interlobe space and the rotors mesh to trap the gas and isolate it from the suction. The rotors' meshing point moves axially from the inlet to the discharge end. The volume of the gas is constantly reduced along this path resulting in a pressure increase. As the gas moves axially, the next charge of gas is drawn into the machine, thus continuing the process. However, the application of screw compressors requires conjugation of the male and female rotors to avoid a gas loss, which means generation of both rotors, must be accomplished with high precision.

The basic geometry of screw rotor profiles has traditionally been given by some kind of ''original generating curves,'' consisting of points, straight lines and points along mathematical curves mixed in suitable proportions. Because compressors must form sealed cavities, multiple contact points usually exist along the cross section during the period of meshing. That is, the ''original generating curves'' and the ''generated curves'' always have to be distributed at cross-sectional profiles for both male and female rotors to keep them well meshed with each other. This condition makes the synthesis of rotor profiles become a difficult work when the criteria of the curve continuity and tangent continuity are requiring satisfied. Mu and Cao [1] proposed an ''accumulative chord cubic parametric spline curve method'' for optimum design of the profile, and presented a ''profile normal line method'' for calculating the conjugate profiles and intermeshing curves. Edstorm [2] and Tang and Fleming [3] used data points to synthesize the rotor profiles. The literature [4,5,6,7] presented some results about how the geometrical parameters of profiles affect the performance of screw compressors. Stosic and Hanjalic [8,9] presented an algorithm of rotor profile curves for specifying screw machine geometry. However, they provided few complete solutions and detailed syntheses of rotor profiles.

In gearing theory, two conjugate curves or surfaces should satisfy the equation of meshing: the relative velocity between two conjugate curves or surfaces is perpendicular to the common normal at the contact point; i.e., they are neither separated nor embedded to each other. In order to obtain the function of the conjugate (generated) curve or surface, the equation of meshing sometimes can be simplified by letting one of the parameter be expressed as an explicit function of other parameters. Then, the equation substitutes the parameter by the explicit function into the function of the conjugate (generated) curve or surface. After the procedure, the ''analytical form'' of the generated curve or surface can then be decided. However, not all the equations of meshing can be simplified like that way; that is, the conjugate curve or surface should be solved simultaneously by using symbolic technique from the equation of meshing and the equations derived from the coordinate transformations about the original generating curves. Apparently, the later one is more complicated than the former one when solving the conjugate (generated) curves or surfaces.

Litvin and Feng [10] presented an analysis and synthesis method of rotor profiles for screw compressors. Their male rotor profile consisted of one elliptical curve and two epicycloidal curves generated by tip points on the female rotor. However, the epicycloidal curve could be derived by simple coordinate transformation of points, and its analytical form for synthesis of the rotor profile can be derived. In this paper, a different rotor profile [11] is examined; multiple original generating curves and generated curves are distributed along cross-sectional profiles of both rotors, where the generated curves can be expressed only by coordinate transformation results and equations of meshing simultaneously. The values of parameters for the original generating curves become difficult to determine since one must make sure that all the generating and generated ones are connected and are in continuous tangency, i.e., singular points must be avoided. This task has been accomplished by trial and error in the past. The present study provides a detailed and theoretically grounded method for profile generation and synthesis. Its systematic determination of values for geometrical parameters can be applied to optimizing and designing new screw-rotor profiles.

2 Generation of Rotor Cross-Sectional Profiles

In this study, the profile in [11] as shown in Fig. 1(*a*) is taken as an example. Fig. 1(*b*) shows magnification of the curves on one tooth.

2.1 Applied Coordinate Systems. Consider the meshing of rotor profiles as the meshing of two planar curves represented by the rotors' cross-section. Coordinate systems S_a, S_b, and S_f are rigidly connected to the male rotor, female rotor and the frame, respectively, as shown in Fig. 2. Both rotors rotate about parallel axes with a constant ratio m_{21} of angular velocities. The centrodes of the rotors are circles of radii r_{mb1} and r_{ft2} that can be represented by the equations

$$r_{ft2}=\frac{C}{1+m_{21}}, \quad r_{mb1}=\frac{Cm_{21}}{1+m_{21}}, \tag{1}$$

Contributed by the Design Automation Committee for publication in the JOURNAL OF MECHANICAL DESIGN. Manuscript received June 1998. Associated Technical Editor: M. A. Ganter.

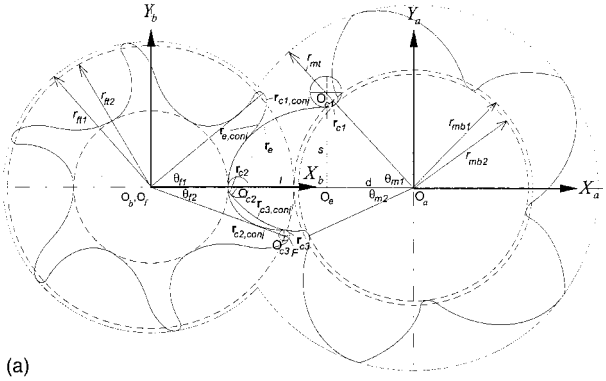

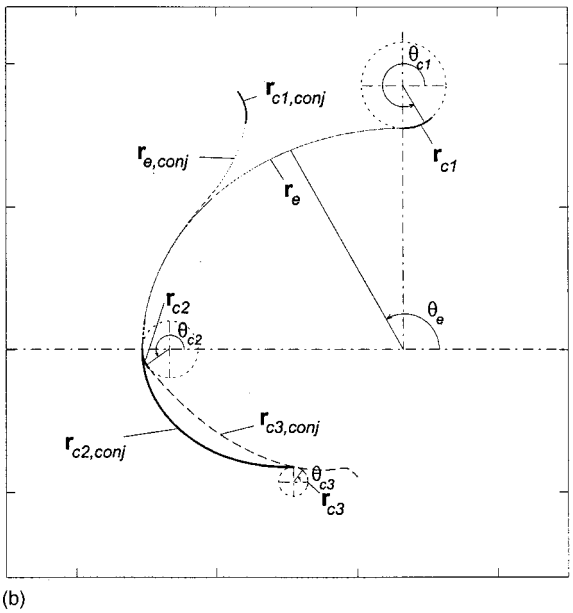

Fig. 1 (*a*) Geometry of rotor profiles in [11]; (*b*) Rotor profile curves

where C is the central distance between the two parallel rotary axes passing through O_a and O_b respectively. Here

$$m_{21}=\frac{\omega_2}{\omega_1}=\frac{\phi_2}{\phi_1}=\frac{N_1}{N_2}, \tag{2}$$

where N_1 and N_2 are the numbers of ''teeth,'' ϕ_1 and ϕ_2 are the angular displacements, ω_1 and ω_2 are the angular velocities of the male rotor and the female rotor, respectively.

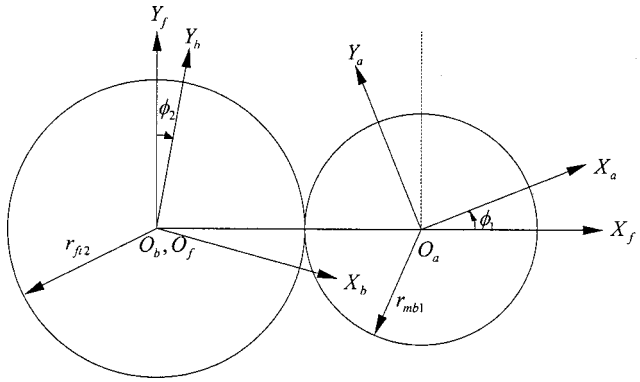

Fig. 2 Coordinate systems for derivation of cross-sectional conjugate rotor profiles

The male rotor has five helical lobes and a like number of helical grooves. Relative to its contacting with the female rotor, it has a pitch circle $\mathbf{r}_{mb1}$ and a rotary axis O_a. The female rotor has six ribs with a pitch circle $\mathbf{r}_{ft2}$ and a rotary axis O_b. The male rotor consists of three original generating curves $\mathbf{r}_{c1}^{(a)}$, $\mathbf{r}_{e}^{(a)}$, $\mathbf{r}_{c2}^{(a)}$ and one generated curve $\mathbf{r}_{c3,conj}^{(a)}$. The female rotor consists of one original generating curve $\mathbf{r}_{c3}^{(b)}$ and three generated curves $\mathbf{r}_{c1,conj}^{(b)}$, $\mathbf{r}_{e,conj}^{(b)}$, and $\mathbf{r}_{c2,conj}^{(b)}$, as shown in Fig. 1. The superscript (*a*) or (*b*) means the vector function is described in the coordinate system S_a or S_b. $\mathbf{r}_{c1}^{(a)}$, $\mathbf{r}_{c2}^{(a)}$, and $\mathbf{r}_{c3}^{(b)}$ are circular arcs with centers at O_{c1}, O_{c2}, and O_{c3}, respectively; $\mathbf{r}_{e}^{(a)}$ is part of an ellipse and makes the end of $\mathbf{r}_{e}^{(a)}$ continuously tangent to $\mathbf{r}_{c1}^{(a)}$ and $\mathbf{r}_{c2}^{(a)}$; $\mathbf{r}_{e,conj}^{(b)}$, $\mathbf{r}_{c1,conj}^{(b)}$, $\mathbf{r}_{c2,conj}^{(b)}$, and $\mathbf{r}_{c3,conj}^{(a)}$ are the ''generated curves'' meshing with $\mathbf{r}_{e}^{(a)}$, $\mathbf{r}_{c1}^{(a)}$, $\mathbf{r}_{c2}^{(a)}$, and $\mathbf{r}_{c3}^{(b)}$, respectively.

2.2 Equations for Elliptical Curve $\mathbf{r}_e$ of Male Rotor. The equation of the elliptical curve $\mathbf{r}_{e}^{(a)}$ is represented in S_a as shown in Fig. 1.

$$\mathbf{r}_{e}^{(a)}(\theta_e)=[l\cos\theta_e-d \quad s\sin\theta_e \quad 0]^T, \quad \left(\frac{\pi}{2}\leqslant\theta_e\leqslant\pi\right), \tag{3}$$

where l and s are the lengths of the longitudinal and latitudinal axes of the ellipse; d is the distance from the ellipse center to the male rotor center O_a; and θ_e is the angular parameter of the ellipse.

The normal vector $\mathbf{N}_{e}^{(a)}$ to $\mathbf{r}_{e}^{(a)}$ is represented in S_a by the equation

$$\mathbf{N}_{e}^{(a)}=[s\cos\theta_e \quad l\sin\theta_e \quad 0]^T. \tag{4}$$

The relative velocity $\mathbf{v}_{12,e}^{(a)}$ can be derived as follows:

$$\begin{aligned}\mathbf{v}_{12,e}^{(a)}&=\mathbf{v}_{1,e}^{(a)}-\mathbf{v}_{2,e}^{(a)}\\&=(\boldsymbol{\omega}_{12}^{(a)}\times\mathbf{r}_{e}^{(a)})-(\overline{O_aO_b}^{(a)}\times\boldsymbol{\omega}_{2}^{(a)})\\&=\begin{bmatrix}\mathbf{i}^{(a)}&\mathbf{j}^{(a)}&\mathbf{k}^{(a)}\\0&0&\omega_1+\omega_2\\l\cos\theta_e-d&s\sin\theta_e&0\end{bmatrix}\\&\quad-\begin{bmatrix}\mathbf{i}^{(a)}&\mathbf{j}^{(a)}&\mathbf{k}^{(a)}\\-C\cos\phi_1&C\sin\phi_1&0\\0&0&-\omega_2\end{bmatrix}\\&=\omega_1[(-(1+m_{21})s\sin\theta_e+Cm_{21}\sin\phi_1]\mathbf{i}^{(a)}\\&\quad+\omega_1[-d(1+m_{21})+l\cos\theta_e(1+m_{21})+Cm_{21}\cos\phi_1]\mathbf{j}^{(a)}.\end{aligned} \tag{5}$$

According to the theory of gearing [12,13], the equation of meshing can be determined by

$$f_e(\theta_e,\phi_1)=\mathbf{N}_{e}^{(a)}\cdot\mathbf{v}_{12,e}^{(a)}=0, \tag{6}$$

where ϕ_1 is the rotation angles of the male rotor. Equations (4), (5), and (6) yield

$$\begin{aligned}f_e(\phi_e,\phi_1)=&[-ld+(l^2-s^2)\cos\theta_e]\sin\theta_e+r_{mb1}(l\cos\phi_1\sin\theta_e\\&+s\sin\phi_1\cos\theta_e)=0,\end{aligned} \tag{7}$$

where r_{mb1} is the pitch circle radius of the male rotor as expressed in Eq. (1).

Using the coordinate transformation from S_a to S_b, the family of elliptical curves is represented in S_b. Considering the family of elliptical curves and the equation of meshing simultaneously, profile $\mathbf{r}_{e,conj}^{(b)}$ of the cross-section of the female rotor is determined in S_b using the equations

$$\mathbf{r}_{e,conj}^{(b)}(\theta_e,\phi_1)=\mathbf{M}_{ba}(\phi_1)\mathbf{r}_{e}^{(a)}(\theta_e), \quad f_e(\theta_e,\phi_1)=0 \tag{8}$$

where matrix

$$\mathbf{M}_{ba}(\phi_1)=\mathbf{M}_{bf}\cdot\mathbf{M}_{fa}=\begin{bmatrix}\cos\phi_2 & -\sin\phi_2 & 0\\ \sin\phi_2 & \cos\phi_2 & 0\\ 0 & 0 & 1\end{bmatrix}\cdot\begin{bmatrix}\cos\phi_1 & -\sin\phi_1 & C\\ \sin\phi_1 & \cos\phi_1 & 0\\ 0 & 0 & 1\end{bmatrix}$$
$$=\begin{bmatrix}\cos[(1+m_{21})\phi_1] & -\sin[(1+m_{21})\phi_1] & C\cos(m_{21}\phi_1)\\ \sin[(1+m_{21})\phi_1] & \cos[(1+m_{21})\phi_1] & C\sin(m_{21}\phi_1)\\ 0 & 0 & 1\end{bmatrix}, \tag{9}$$

describes the coordinate transformation in transition from S_a to S_b, as shown in Fig. 2, and the subscript *conj* means the ''conjugate shape.''

2.3 Equations of Circular Arcs $\mathbf{r}_{c1}$ and $\mathbf{r}_{c2}$ of Male Rotor. Equation of circular arcs $\mathbf{r}_{c1}^{(a)}$ and $\mathbf{r}_{c2}^{(a)}$ are represented in S_a, as shown in Fig. 1,

$$\mathbf{r}_i^{(a)}(\theta_i)=[r_i\cos\theta_i+x_i \quad r_i\sin\theta_i+y_i \quad 0]^T, \quad (i=c1,c2) \tag{10}$$

where r_i is the radius of $\mathbf{r}_i^{(a)}$ and (x_i,y_i) is the coordinate of center O_{c1} or O_{c2} described in the coordinate system S_a for the circular arc $\mathbf{r}_i^{(a)}$, respectively; θ_i is the angular parameter of the circular arc.

The normal vector $\mathbf{N}_i^{(a)}$ to $\mathbf{r}_i^{(a)}$ is represented in S_a by the equation

$$\mathbf{N}_i^{(a)}=[r_i\cos\theta_i \quad r_i\sin\theta_i \quad 0]^T. \tag{11}$$

The relative velocity $\mathbf{v}_{12,i}^{(a)}$ can be derived as following:

$$\begin{aligned}\mathbf{v}_{12,i}^{(a)}&=\mathbf{v}_{1,i}^{(a)}-\mathbf{v}_{2,i}^{(a)}\\ &=(\boldsymbol{\omega}_{12}^{(a)}\times\mathbf{r}_i^{(a)})-(\overline{O_aO_b}^{(a)}\times\boldsymbol{\omega}_2^{(a)})\\ &=\begin{bmatrix}\mathbf{i}^{(a)} & \mathbf{j}^{(a)} & \mathbf{k}^{(a)}\\ 0 & 0 & \omega_1+\omega_2\\ r_i\cos\theta_i+x_i & r_i\sin\theta_i+y_i & 0\end{bmatrix}\\ &\quad-\begin{bmatrix}\mathbf{i}^{(a)} & \mathbf{j}^{(a)} & \mathbf{k}^{(a)}\\ -C\cos\phi_1 & C\sin\phi_1 & 0\\ 0 & 0 & -\omega_2\end{bmatrix}\\ &=\omega_1[-(1+m_{21})(y_i+r_i\sin\theta_i)+Cm_{21}\sin\phi_1]\mathbf{i}^{(a)}\\ &\quad+\omega_1[(1+m_{21})(x_i+r_i\cos\theta_i)+Cm_{21}\cos\phi_1]\mathbf{j}^{(a)}.\end{aligned} \tag{12}$$

The equation of meshing can then be determined using

$$f_i(\theta_i,\phi_1)=\mathbf{N}_i^{(a)}\cdot\mathbf{v}_{12,i}^{(a)}=0. \tag{13}$$

Equations (11), (12), and (13) yield

$$f_i(\theta_i,\phi_1)=-y_i\cos\theta_i+x_i\sin\theta_i+r_{mb1}\sin(\phi_1+\theta_i)=0. \tag{14}$$

Profile $\mathbf{r}_{i,conj}^{(b)}$ of the cross-section of the female rotor is determined in S_b using the equations

$$\mathbf{r}_{i,conj}^{(b)}(\theta_i,\phi_1)=\mathbf{M}_{ba}(\phi_1)\mathbf{r}_i^{(a)}(\theta_i), \quad f_i(\theta_i,\phi_1)=0, \tag{15}$$

where matrix $\mathbf{M}_{ba}(\phi_1)$ is the same as in Eq. (9).

2.4 Equations of Circular Arc $\mathbf{r}_{c3}$ of the Female Rotor. The equation of circular arc $\mathbf{r}_{c3}^{(b)}$ is represented in S_b, as shown in Fig. 1,

$$\mathbf{r}_{c3}^{(b)}(\theta_{c3})=[r_{c3}\cos\theta_{c3}+x_{c3} \quad r_{c3}\sin\theta_{c3}+y_{c3} \quad 0]^T, \tag{16}$$

where r_{c3} is the radius of $\mathbf{r}_{c3}^{(b)}$ and (x_{c3},y_{c3}) is the coordinate of center O_{c3} for the circular arc $\mathbf{r}_{c3}^{(b)}$.

The normal vector $\mathbf{N}_{c3}^{(b)}$ to $\mathbf{r}_{c3}^{(b)}$ is represented in S_b by the equation

$$\mathbf{N}_{c3}^{(b)}=[r_{c3}\cos\theta_{c3} \quad r_{c3}\sin\theta_{c3} \quad 0]^T. \tag{17}$$

The relative velocity $\mathbf{v}_{12,c3}^{(b)}$ can be derived as following:

$$\begin{aligned}\mathbf{v}_{21,c3}^{(b)}&=\mathbf{v}_{2,c3}^{(b)}-\mathbf{v}_{1,c3}^{(b)}\\ &=(\boldsymbol{\omega}_{21}^{(b)}\times\mathbf{r}_{c3}^{(b)})-(\overline{O_bO_a}^{(b)}\times\boldsymbol{\omega}_1^{(b)})\\ &=\begin{bmatrix}\mathbf{i}^{(b)} & \mathbf{j}^{(b)} & \mathbf{k}^{(b)}\\ 0 & 0 & -\omega_1-\omega_2\\ r_{c3}\cos\theta_{c3}+x_{c3} & r_{c3}\sin\theta_{c3}+y_{c3} & 0\end{bmatrix}\\ &\quad-\begin{bmatrix}\mathbf{i}^{(b)} & \mathbf{j}^{(b)} & \mathbf{k}^{(b)}\\ C\cos\phi_2 & C\sin\phi_2 & 0\\ 0 & 0 & \omega_1\end{bmatrix}\\ &=\omega_1[(1+m_{21})(y_{c3}+r_{c3}\sin\theta_{c3})-Cm_{21}\sin\phi_2]\mathbf{i}^{(b)}\\ &\quad+\omega_1[-(1+m_{21})(x_{c3}+r_{c3}\cos\theta_{c2})+Cm_{21}\cos\phi_2]\mathbf{j}^{(b)}.\end{aligned} \tag{18}$$

In accordance with the theorem of gearing, the equation of meshing can be determined using

$$f_{c3}(\theta_{c3},\phi_2)=\mathbf{N}_{c3}^{(b)}\cdot\mathbf{v}_{21,c3}^{(b)}=0, \tag{19}$$

where ϕ_2 is the rotation angle of the female rotor. Equations (17), (18), and (19) yield

$$f_{c3}(\theta_{c3},\phi_2)=y_{c3}\cos\theta_{c3}-x_{c3}\sin\theta_{c3}+r_{ft2}\sin(\theta_{c3}-\phi_2)=0. \tag{20}$$

Profile $\mathbf{r}_{c3,conj}^{(a)}$ of the cross-section of the male rotor is determined in S_a using the equations

$$\mathbf{r}_{c3,conj}^{(a)}(\theta_{c3},\phi_2)=\mathbf{M}_{ab}(\phi_2)\mathbf{r}_{c3}^{(b)}(\theta_{c3}), \quad f_{c3}(\theta_{c3},\phi_2)=0, \tag{21}$$

where matrix

$$\mathbf{M}_{ab}(\phi_2)=\mathbf{M}_{af}\cdot\mathbf{M}_{fb}=\begin{bmatrix}\cos\phi_1 & \sin\phi_1 & -C\cos\phi_1\\ -\sin\phi_1 & \cos\phi_1 & C\cos\phi_1\\ 0 & 0 & 1\end{bmatrix}\cdot\begin{bmatrix}\cos\theta_2 & \sin\phi_2 & 0\\ -\sin\theta_2 & \cos\phi_2 & 0\\ 0 & 0 & 1\end{bmatrix}$$

$$=\begin{bmatrix}\cos\left[\left(1+\frac{1}{m_{21}}\right)\phi_2\right] & \sin\left[\left(1+\frac{1}{m_{21}}\right)\phi_2\right] & -C\cos\left(\frac{\phi_2}{m_{21}}\right)\\ -\sin\left[\left(1+\frac{1}{m_{21}}\right)\phi_2\right] & \cos\left[\left(1+\frac{1}{m_{21}}\right)\phi_2\right] & C\sin\left(\frac{\phi_2}{m_{21}}\right)\\ 0 & 0 & 1\end{bmatrix}. \quad (22)$$

describes the coordinate transformation in transition from S_b to S_a (Fig. 2).

3 Synthesis of Cross-Sectional Profiles of Rotors

The equations for the original generating curves and the generated curves can be determined according to the foregoing derivation. However, from a design stand point, it is difficult to determine which geometrical parameters should be determined at first and which should then be derived, especially since the radius of r_{c3} affects whether the end points of $\mathbf{r}_{c3,conj}$ and $\mathbf{r}_{c2}$ intersect and remain continuously tangent. Continuity at the intersection points of the $\mathbf{r}_{c2,conj}$ and $\mathbf{r}_{c3}$ must also be considered at the same time. The bound values for all profile parts and the bound values of kinematic parameters are also considered in this study. The optimization tool can be applied to get improved parametric values for these profiles automatically after the systematic parameter setting is done.

The geometric parameter values that must be given first are: (Fig. 1)

1 N_1, N_2: male and female rotor tooth numbers, respectively;
2 C: center distance between male and female rotor rotary axes;
3 l,s: longitudinal and latitudinal axial lengths of the ellipse $\mathbf{r}_e$, respectively;
4 r_{c2}: radius of the circular arc $\mathbf{r}_{c2}$;
5 θ_{m1}: initial angle of the ''tooth'' on the male rotor;
6 d: distance from ellipse center to male rotor center O_1.

The other geometric values can then be determined step-by-step as follows:

Step 1. Parameters of circular arc $\mathbf{r}_{c1}$

From Fig. 1, the radius of $\mathbf{r}_{c1}$ can be determined using

$$r_{c1}=\frac{\sin\theta_{m1}\times d}{\cos\theta_{m1}}-s \quad (23)$$

and

$$\frac{3\pi}{2}<\theta_{c1}<2\pi-\theta_{m1}. \quad (24)$$

Step 2. Parameters of circular arcs $\mathbf{r}_{c2}$ *and* $\mathbf{r}_{c3}$

According to Eq. (15), the equation for the generated curve $\mathbf{r}^{(b)}_{c2,conj}$ can be written as

$$\mathrm{r}^{(b)}_{c2,conj}=[x_{c2,conj}(\theta_{c2},\phi_1)\quad y_{c2,conj}(\theta_{c2},\phi_1)\quad 0]^T \quad (25)$$

and

$$f_{c2}(\theta_{c2},\phi_1)=0. \quad (26)$$

Take the derivative of Eq. (26) using ϕ_1,

$$\frac{df_{c2}}{d\phi_1}=\frac{\partial f_{c2}}{\partial\phi_1}+\frac{\partial f_{c2}}{\partial\theta_{c2}}\frac{\partial\theta_{c2}}{\partial\phi_1}=0, \quad (27)$$

then

$$\frac{\partial\theta_{c2}}{\partial\phi_1}=\frac{-\frac{f_{c2}}{\partial\phi_1}}{\frac{\partial f_{c2}}{\partial\theta_{c2}}}. \quad (28)$$

The tangent $\mathbf{t}^{(b)}_{c2,conj}$ of $\mathbf{r}^{(b)}_{c2,conj}$ can be represented as:

$$\mathbf{t}^{(b)}_{c2,conj}=\begin{bmatrix}\frac{dx_{c2,conj}}{d\phi_1} & \frac{dy_{c2,conj}}{d\phi_1} & 0\end{bmatrix}^T, \quad (29)$$

where

$$\frac{dx_{c2,conj}}{d\phi_1}=\frac{\partial x_{c2,conj}}{\partial\phi_1}+\frac{\partial x_{c2,conj}}{\partial\theta_{c2}}\frac{\partial\theta_{c2}}{\partial\phi_1}, \quad (30)$$

$$\frac{dy_{c2,conj}}{d\phi_1}=\frac{\partial y_{c2,conj}}{\partial\phi_1}+\frac{\partial y_{c2,conj}}{\partial\theta_{c2}}\frac{\partial\theta_{c2}}{\partial\phi_1}. \quad (31)$$

Substituting Eq. (28) into (30) and (31) allows the tangent $\mathbf{t}^{(b)}_{c2,conj}$ be determined.

The normal vector $\mathbf{N}^{(b)}_{c2,conj}$ of the $\mathbf{r}^{(b)}_{c2,conj}$ can also be determined using

$$\mathbf{N}^{(b)}_{c2,conj}=\begin{bmatrix}\frac{dy_{c2,conj}}{d\phi_1} & -\frac{dx_{c2,conj}}{d\phi_1} & 0\end{bmatrix}^T. \quad (32)$$

So the line perpendicular to $\mathbf{r}^{(b)}_{c2,conj}$ can be represented as

$$(X-x^{(b)}_{c2,conj})\frac{dx^{(b)}_{c2,conj}}{d\phi_1}+(Y-y^{(b)}_{c2,conj})\frac{dy^{(b)}_{c2,conj}}{d\phi_1}=0. \quad (33)$$

According to the description of [11], the center O_{c3} of circular arc $\mathbf{r}^{(b)}_{c3}$ should be located on the limiting ray between the female rotor center O_b and the tip point $F:(x_{ft},y_{ft})$ of the female rotor, as shown in Fig. 3. The limiting ray can be represented as

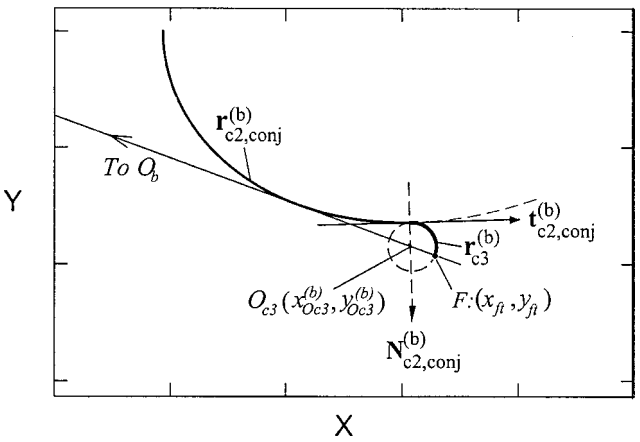

Fig. 3 Geometry of rotor profiles around O_{c3}

Table 1 The parameter values of the cross-sectional rotor profiles

Symbol	Value
θ_{m1}	48.0
θ_{m2}	24.0*
θ_{f1}	40.0*
θ_{f2}	20.0*
l	37.33
s	31.00
d	33.33
C	100.00
r_{mt}	70.66*
r_{p1}	54.54*
r_{p2}	45.45*
r_{mb1}	45.45*
r_{mb2}	43.79*
r_{ft1}	56.20*
r_{ft2}	54.55*
r_{c1}	6.02*
r_{c2}	4.00
r_{c3}	2.07*

Position	x	y
$O_{c1}^{(a)}$	-33.33*	37.02*
$O_{c2}^{(a)}$	-66.66	0.00
$O_{c3}^{(b)}$	50.86*	-18.51*
Geometry parameters	θ_{lower}	θ_{upper}
θ_{ellipe}	90°	180°
θ_{rc1}	270°	312°*
θ_{rc2}	180°	219.07°*
θ_{rc3}	-20°*	91.32°*
Kinematic parameters	ϕ_{lower}	ϕ_{upper}
$\phi_{ellipe}^{(a)}$	0°*	42.834°*
$\phi_{rc1}^{(a)}$	42.834°*	48°*
$\phi_{rc2}^{(a)}$	0°*	28.505°*
$\phi_{rc3}^{(a)}$	-24°*	28.505°*

Unit = mm or degree

Note: * is denotes that the value is derived.

$$Y=\tan(-\theta_{f2})X. \tag{34}$$

To keep the generated curve $\mathbf{r}_{c2,conj}^{(b)}$ on the female rotor continuous and tangent to $\mathbf{r}_{c3}^{(b)}$, the center $O_{c3}:(x_{Oc3}^{(b)},y_{Oc3}^{(b)})$ of circular arc $\mathbf{r}_{c3}^{(b)}$ should satisfy the condition that the distances from O_{c3} to F and from O_{c3} to $\mathbf{r}_{c2,conj}^{(b)}$ be equal, that is,

$$r_{c3}^2=(X-x_{ft})^2+(Y-y_{ft})^2=(X-x_{c2,conj}^{(b)})^2+(Y-y_{c2,conj}^{(b)})^2, \tag{35}$$

where r_{c3} is the radius of circular arc $\mathbf{r}_{c3}^{(b)}$.

The 4 unknowns: X,Y,θ_{c2},ϕ_1 can then be determined by solving Eqs. (33), (34), (35) and (26) simultaneously, then

$$(x_{0c3}^{(b)},y_{Oc3}^{(b)})=(X,Y), \tag{36}$$

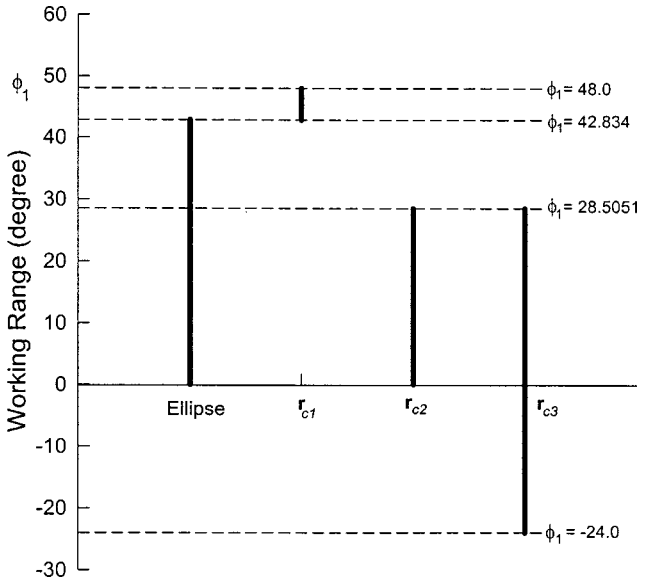

Fig. 4 Working ranges for every part of the curve profile

and

$$\theta_{c2,upper}=\theta_{c2}, \tag{37}$$

where $\theta_{c2,upper}$ is the upper bound of θ_{c2}, so,

$$\pi<\theta_{c2}\leqslant\theta_{c2,upper}. \tag{38}$$

The resulting ϕ_1 can then be used to determine the upper bound: $\theta_{c3,upper}$ of the $\mathbf{r}_{c3}^{(b)}$ by substituting $\phi_2=m_{21}\phi_1$ into $f_{c3}(\theta_{c3},\phi_2)=0$ and solving for θ_{c3}, thusly

$$-\theta_{f2}\leqslant\theta_{c3}\leqslant\theta_{c3,upper}. \tag{39}$$

The radius of $\mathbf{r}_{c3}^{(b)}$ can also be determined as follows:

$$r_{c3}=\sqrt{(x_{Oc3}^{(b)}-x_{ft})^2+(y_{Oc3}^{(b)}-y_{ft})^2}. \tag{40}$$

The above analysis shows how all the geometric parameter values listed in Table 1 are systematically derived. The kinematic parameter ϕ_1 can also be determined by solving meshing equations for every part of the curves, since θ_j is known, where subscript j represents *e, c1, c2,* and *c3,* respectively. The ranges of ϕ_1's for every curve defined as ''working range'' mean that the curve is in mesh when the rotors are rotating within these ranges, and the results are shown as figure in Fig. 4. It can be seen that there are three contact points simultaneously located on $\mathbf{r}_e$, $\mathbf{r}_{c2}$, and $\mathbf{r}_{c3}$ within $0°\leqslant\phi_1\leqslant28.505°$, respectively, and only one contact point in the other ranges when only one period of tooth-meshing is considered.

4 Generation of Rotor Surfaces

4.1 Applied Coordinate Systems. Movable coordinate systems, S_1 and S_2, are rigidly connected to Rotor 1 and Rotor 2 (Fig. 5). The fixed coordinate system S_f is rigidly connected to the frame of the compressor.

4.2 Equations for the Rotor Surfaces. The rotor surface may be obtained by performing a screw motion on the cross-sectional profile of the rotor about the rotor axis. Then, Rotor 1 will be provided with surfaces $\Sigma_e^{(1)}$, $\Sigma_{c1}^{(1)}$, and $\Sigma_{c2}^{(1)}$ represented by the equations

$$\mathbf{r}_j^{(1)}(\theta_j,\psi_1)=\mathbf{M}_{1a}(\psi_1)\mathbf{r}_j^{(a)}(\theta_j),\quad (j=e,c1,c2), \tag{41}$$

and $\Sigma_{c3}^{(2)}$ on Rotor 2 is represented as

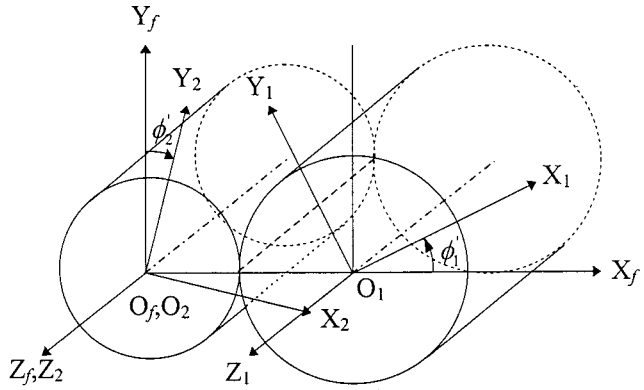

Fig. 5 Coordinate systems for Rotor 1 and Rotor 2

$$\mathbf{r}_{c3}^{(2)}(\theta_{c3},\psi_1)=\mathbf{M}_{2b}(\psi_1)\mathbf{r}_{c3}^{(b)}(\theta_{c3}), \tag{42}$$

where matrices

$$\mathbf{M}_{1a}=\begin{bmatrix}\cos\psi_1 & \sin\psi_1 & 0 & 0\\ -\sin\psi_1 & \cos\psi_1 & 0 & 0\\ 0 & 0 & 1 & -h_1\psi_1\\ 0 & 0 & 0 & 1\end{bmatrix} \tag{43}$$

and

$$\mathbf{M}_{2b}=\begin{bmatrix}\cos\psi_1 & -\sin\psi_1 & 0 & 0\\ \sin\psi_1 & \cos\psi_1 & 0 & 0\\ 0 & 0 & 1 & -h_2\psi_1\\ 0 & 0 & 0 & 1\end{bmatrix} \tag{44}$$

describe the coordinate transformation in transition from S_a to S_1 and from S_b to S_2, as shown in Fig. 6(a) and Fig. 6(b); h_1 and $h_2=h_1/m_{21}$ are the screw parameters of Rotor 1 and Rotor 2, respectively. Subscript j indicates the surface is generated by the parts of ellipse *e*, circular arc *c1*, circular arc *c2* of the Rotor 1, and circular arc *c3* of the Rotor 2, respectively.

The normal to $\Sigma_j^{(1)}$ represented in S_1 and the normal to $\Sigma_{c3}^{(2)}$ represented in S_2 are

$$\mathbf{N}_j^{(1)}=\frac{\partial\mathbf{r}_j^{(1)}}{\partial\theta_j}\times\frac{\partial\mathbf{r}_j^{(1)}}{\partial\psi_1}, \tag{45}$$

and

$$\mathbf{N}_{c3}^{(2)}=\frac{\partial\mathbf{r}_{c3}^{(2)}}{\partial\theta_{c3}}\times\frac{\partial\mathbf{r}_{c3}^{(2)}}{\partial\psi_1}. \tag{46}$$

The relative velocity

$$\begin{aligned}\mathbf{v}_{12,j}^{(1)}&=\mathbf{v}_{1,j}^{(1)}-\mathbf{v}_{2,j}^{(1)}\\ &=(\boldsymbol{\omega}_{12}^{(1)}\times\mathbf{r}_j^{(1)})-(\overline{O_1O_2}^{(1)}\times\boldsymbol{\omega}_2^{(1)})\\ &=\begin{bmatrix}\mathbf{i}^{(1)} & \mathbf{j}^{(1)} & \mathbf{k}^{(1)}\\ 0 & 0 & \omega_1+\omega_2\\ x_j & y_j & z_j\end{bmatrix}-\begin{bmatrix}\mathbf{i}^{(1)} & \mathbf{j}^{(1)} & \mathbf{k}^{(1)}\\ -C\cos\phi_1' & C\sin\phi_1' & 0\\ 0 & 0 & -\omega_2\end{bmatrix}\end{aligned} \tag{47}$$

can be determined, and the relative velocity

$$\begin{aligned}\mathbf{v}_{21,c3}^{(2)}&=\mathbf{v}_{2,c3}^{(2)}-\mathbf{v}_{1,c3}^{(2)}\\ &=(\boldsymbol{\omega}_{21}^{(2)}\times\mathbf{r}_{c3}^{(2)})-(\overline{O_2O_1}^{(2)}\times\boldsymbol{\omega}_1^{(2)})\\ &=\begin{bmatrix}\mathbf{i}^{(2)} & \mathbf{j}^{(2)} & \mathbf{k}^{(2)}\\ 0 & 0 & -\omega_1-\omega_2\\ x_{c3} & y_{c3} & z_{c3}\end{bmatrix}-\begin{bmatrix}\mathbf{i}^{(2)} & \mathbf{j}^{(2)} & \mathbf{k}^{(2)}\\ C\cos\phi_2' & C\sin\phi_2' & 0\\ 0 & 0 & \omega_1\end{bmatrix}\end{aligned} \tag{48}$$

can also be determined. Where ϕ_1' and ϕ_2' are the angles of rotation of Rotor 1 and Rotor 2 in the meshing process of Rotors 1 and 2, respectively, as shown in Fig. 5. Equations (45)–(48) can then be used to yield the equations of meshing:

$$F_j(\theta_j,\phi_1',\psi_1)=\mathbf{N}_j^{(1)}\cdot v_{12,j}^{(1)}=0, \tag{49}$$

and

$$F_{c3}(\theta_{c3},\phi_2',\psi_1)=\mathbf{N}_{c3}^{(2)}\cdot v_{21,c3}^{(2)}=0. \tag{50}$$

In the same way, the generated surface $\Sigma_{c3,conj}^{(1)}$ of Rotor 1 represented in S_1 and the surfaces $\Sigma_{e,conj}^{(2)}$, $\Sigma_{c1,conj}^{(2)}$, and $\Sigma_{c2,conj}^{(2)}$ of Rotor 2 represented in S_2 can be expressed by the equations:

$$\begin{aligned}&\mathbf{r}_{c3,conj}^{(1)}(\theta_{c3},\phi_2',\psi_1)=\mathbf{M}_{12}(\phi_2')\cdot\mathbf{M}_{2b}(\psi_1)\cdot\mathbf{r}_{c3}^{(b)}(\theta_{c3}),\\ &F_{c3}(\theta_{c3},\phi_2',\psi_1)=0,\end{aligned} \tag{51}$$

and

$$\begin{aligned}&\mathbf{r}_{j,conj}^{(2)}(\theta_j,\phi_j',\psi_1)=\mathbf{M}_{21}(\phi_1')\cdot\mathbf{M}_{1a}(\psi_1)\cdot\mathbf{r}_j^{(a)}(\theta_j),\\ &F_j(\theta_j,\phi_1',\psi_1)=0,\quad (j=e,c1,c2),\end{aligned} \tag{52}$$

where the subscript *conj* indicates the surface is the conjugate shape; θ_j, θ_{c3}, ϕ_1', ϕ_2', and ψ_1 are the surface parameters.

The above derivation shows how the complete surfaces of both rotors, as shown in Fig. 7, can be determined.

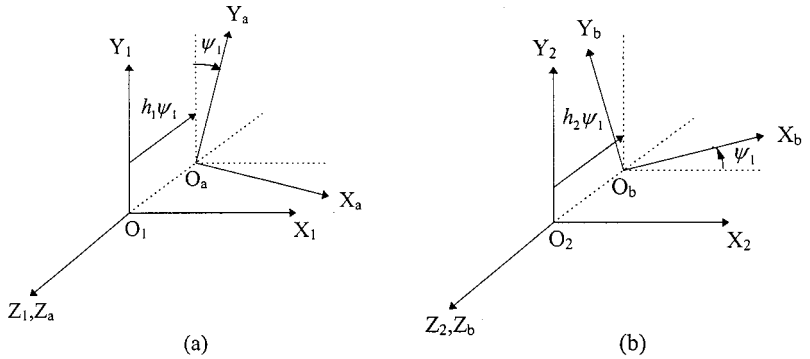

Fig. 6 (a) Generation mechanism for Rotor 1 surfaces; (*b*) Generation mechanism for Rotor 2 surfaces

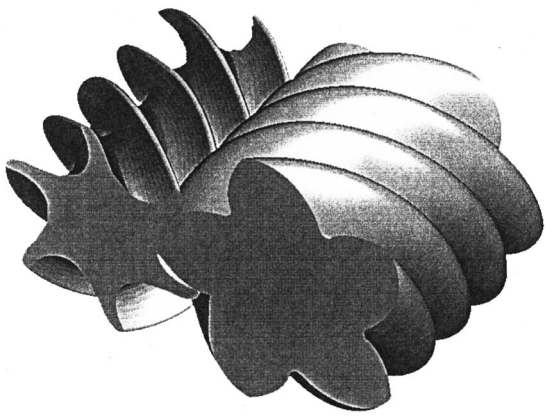

Fig. 7 Surfaces of twin-screw compressor rotors

4.3 Contact Lines on Rotor Surfaces. The contact lines between two mating rotor surfaces on rotor surface 1 are determined as

$$\mathbf{r}_j^{(1)}(\theta_j,\psi_1),\quad F_j(\theta_j,\phi_1',\psi_1)=0\quad (j=e,c1,c2). \tag{53}$$

The family of contact lines on rotor surface 1 can be obtained by considering various values of ϕ_1'. In addition to these contact lines, there are contact lines on $\Sigma_{c3,conj}^{(1)}$, and they can be determined using:

$$\mathbf{r}_{c3,conj}^{(1)}(\theta_{c3},\phi_2,\psi_1),\quad F_{c3}(\theta_{c3},\phi_2',\psi_1)=0. \tag{54}$$

Substituting ϕ_2' by ϕ_2 into Eq. (50) allows the contact lines on $\Sigma_{c3,conj}^{(1)}$ to be obtained. The complete contact lines of different rotation angles 0 deg, 15 deg, and 30 deg on the male rotor are shown in Fig. 8, respectively.

The contact lines on surface of Rotor 2 are determined using

$$\mathbf{r}_{c3}^{(2)}(\theta_{c3},\psi_1),\quad F_{c3}(\theta_{c3},\phi_2',\psi_1)=0. \tag{55}$$

The family of contact lines on rotor surface 2 can be obtained by considering various values of ϕ_2'. In addition to these contact lines, there are contact lines on $\Sigma_{j,conj}^{(2)}$ and they can be determined by:

$$\mathbf{r}_{j,conj}^{(2)}(\theta_j,\phi_1,\psi_1),\quad F_j(\theta_j,\phi_1',\psi_1)=0,\quad (j=e,c1,c2). \tag{56}$$

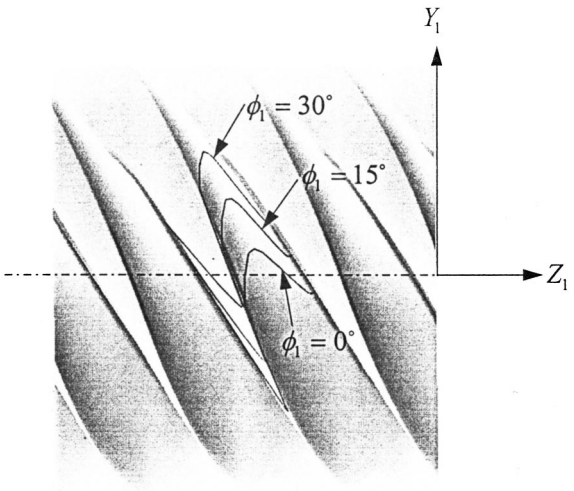

Fig. 8 Contact lines on male rotor surface

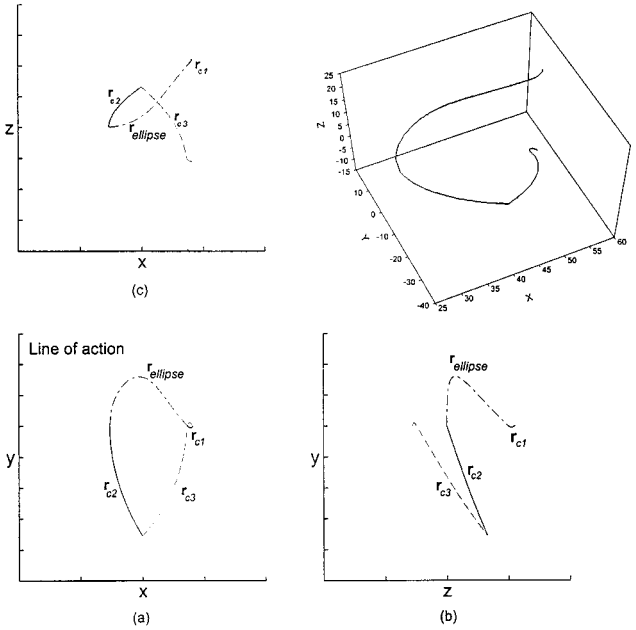

Fig. 9 Contact line projections

Substituting ϕ_1' by ϕ_1 into Eq. (52) allows the contact lines on $\Sigma_{j,conj}^{(2)}$ to be obtained.

4.4 Line of Action. The projection of contact lines from the end view (on the X_f-Y_f plane) can be determined by transforming contact points into the fixed coordinate system S_f, as shown in Fig. 9(a). They are the so-called the lines of action and can be determined using following equations:

$$\mathbf{r}_j^{(f)}(\theta_j,\phi_1)=\mathbf{M}_{fa}(\phi_1)\mathbf{r}_j^{(a)}(\theta_j),\quad f_j(\theta_j,\phi_1)=0\quad (j=e,c1,c2) \tag{57}$$

and

$$\mathbf{r}_{c3}^{(f)}(\theta_{c3},\phi_2)=\mathbf{M}_{fb}(\phi_2)\mathbf{r}_{c3}^{(b)}(\theta_{c3}),\quad f_{c3}(\theta_{c3},\phi_2)=0. \tag{58}$$

The coordinates in Z_f direction can be determined using

$$z^{(f)}=r_{mb1}\times\phi_1\times\tan\lambda, \tag{59}$$

where λ is the lead angle of the rotor and ϕ_1 is the same set derived from Eq. (57) and Eq. (58). Figures 9(b) and 9(c) show the projections of contact lines on the Y_f-Z_f and X_f-Z_f planes, respectively. The different line-types show that the contact lines are on different rotor surface patches. However, the contact line will retain their shapes and translate along the Z_f-axis on the Y_f-Z_f and X_f-Z_f planes when the rotor rotates. Since the coordinates of the points in the line of contact are determined from above equations, the true length of contact line can then be evaluated from the numerical integration method. Furthermore, the length of contact line means the length of leakage line that depends on the profile shapes.

4.5 Blowhole Area Calculation. The blowhole is a small triangular-shaped area formed by the housing cusp and the male and female rotor tips. Figure 10 shows a cross-section of the housing and the two rotors in a plane normal to the rotors axes. One of the male rotor lobes is contacting the bottom housing cusp and the mating rotor, thus creating a leakage path from cavity I to cavity II. The so-called leakage triangle does not lie in a Cartesian plane. It can only properly be defined in curvilinear coordinates. Figure 11 shows the leakage triangle in a typical screw compressor. The leakage triangle can actually be visualized in a simpler way. How-

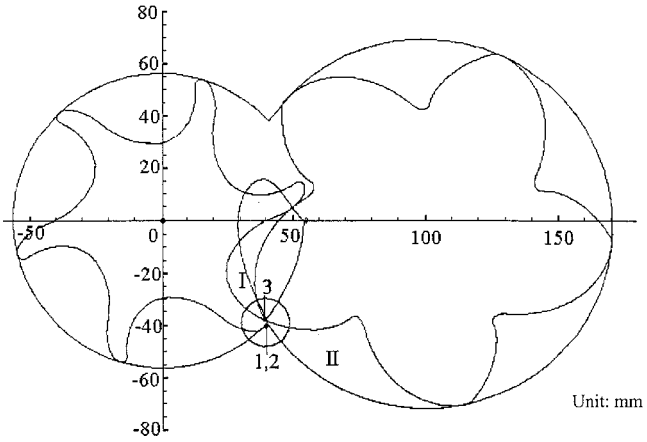

Fig. 10 End-view section through blowhole

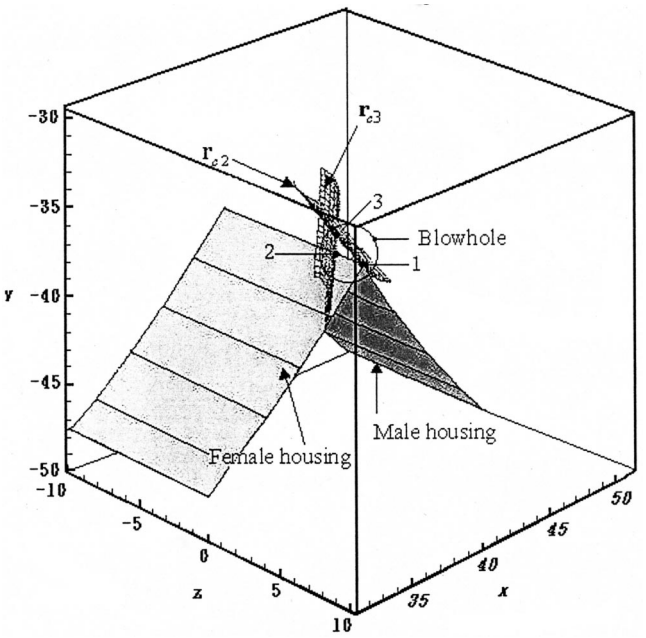

Fig. 11 Definition of leakage triangle

ever, to define the actual blowhole area is complicate. Many papers have discussed the blowhole area definitions and its calculations [5,14–16].

In this paper, three points on the flanks of the rotors and the cusp of the housing define the leakage triangle. The first tip of the leakage triangle lies at the point where the trailing flank of the male rotor is on the verge of separating (point 1 in Figs. 10 and 11). The second tip is defined as the point located on trailing flank of the female rotor that aligns with the lower cusp (point 2 in Figs. 10 and 11). The third tip can be defined by the contact point between two rotors, which is closest to the lower cusp of housing (point 3 in Figs. 10 and 11). After the coordinates of these three points are defined in this study, the blowhole area can then be determined by the numerical methods.

5 Optimum Design of the Rotor Profiles

In this paper, all the equations are derived and simplified automatically by using commercial mathematical software: *Mathematica 3.0* [17]. It provides strong abilities for symbolic and numerical computations. The symbolic expressions for manipulating equations are implemented by hand and the detail expressions of the final equations are not derived. The results for the length of contact line and the blowhole area are evaluated less than 8 minutes in Microsoft NT 4.0 on PC with Pentium 150 and 96M RAM. With the help of the interface coupler [18] between the analysis software *Mathematica 3.0* and the optimization tool *MOST 1.1* [19], the process of optimization can be finished automatically. At the *MOST*, a Sequential Quadratic Programming (SQP) is selected as a single objective optimizer for its accuracy, reliability and efficiency. In this paper, the purpose of the optimization is to reduce the contact-line length and the blowhole area. Three cases are presented here:

Case 1: As the synthesis procedure mentioned above, five variables l, s, r_{c2}, θ_{m1}, and d are chosen as the design variables to minimize the contact line length.

Table 2 and Fig. 12 show the improved results that the contact-line length reduces from 139.63 mm/mesh to 110.85 mm/mesh. However, the blowhole area increases from 6.64 mm^2 to 28.16 mm^2.

Case 2: Similar to case 1, the same five variables l, s, r_{c2}, θ_{m1}, and d are chosen as design variables but to minimize the blowhole area. The improved results are shown in Fig. 13 and Table 2. Notice that the blowhole area reduced from 6.64 mm^2 to 2.63 mm^2, but the contact-line length increases from 139.63 mm/mesh to 146.84 mm/mesh.

From the results of cases 1 and 2, they imply that the contact-line leakage length is likely to increase with the reduction in the blowhole area [14,20]. Both object functions in cases 1 and 2 are conflict with each other. It is a typical multi-objective problem. The constraint method [21] is chosen to formulate the multi-objective problem. The basic idea of the constraint method is to optimize one objective while representing all the other objectives as constraints. Therefore, a single-objective optimization problem can be formulated as the following case.

Table 2 Optimum results for three cases

	Original Design	Case 1	Case 2	Case 3
Objective Function		Contact line length	Blowhole area	Contact line length
Constraint		$r_{c1} \geq 0$	$r_{c1} \geq 0$	Blowhole area ≤ 3.00, $r_{c1} \geq 0$
Design Variables				
l *(mm)*	37.33	35.17	38.53	37.34
s *(mm)*	31.00	31.58	31.59	35.00
r_{c2} *(mm)*	4.00	4.098	3.69	3.192
θ_{m1}	48°	45°	47.25°	48°
d *(mm)*	33.33	31.70	34.18	33.34
Contact Line Length *(mm/mesh)*	139.63	110.85	146.84	124.67
Blowhole Area *(mm^2)*	6.64	28.16	2.63	2.72

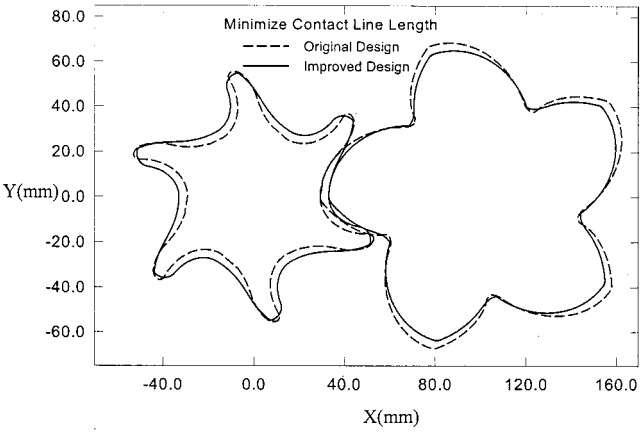

Fig. 12 Optimization result for Case 1

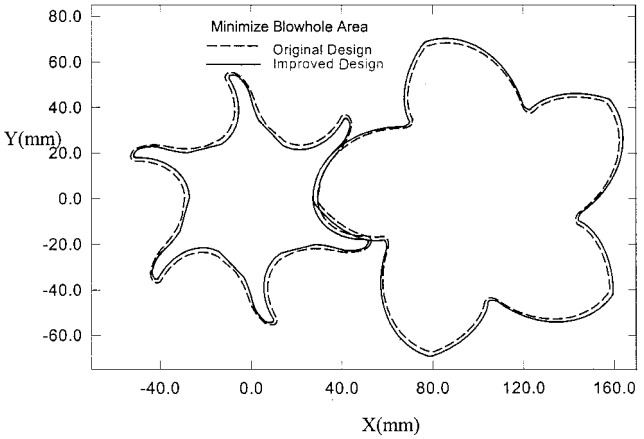

Fig. 13 Optimization result for Case 2

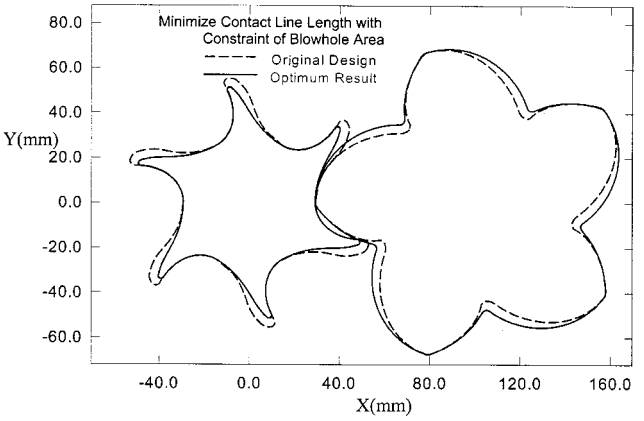

Fig. 14 Optimization result for Case 3

Case 3: Taking the same five variables as design variables, and the formulation of the single-objective optimization problem becomes defining the object function as minimizing the contact-line length subject to the constraint of blowhole area with a limited value 3 mm^2. Figure 14 and Table 2 show the results of optimization. Obviously, the contact-line length is reduced from 139.63 mm/mesh to 124.67 mm/mesh compared with the original design and the blowhole area, 2.72 mm^2, is also satisfying the constraint. Both the contact-line length and the blowhole area in the original design are reduced simultaneously in this case, and it is really useful to fulfill the better performance for screw compressor from the leakage standpoint.

6 Conclusions

This paper derives the complete generation processes for rotor profiles and proposes a systematic synthesis method by using symbolic technique for rotor profiles used in the twin-screw compressors as mentioned in [11]. Commercial mathematical software, *Mathematica 3.0*, is applied to derive and simplify the equations automatically by using its symbolic and numerical computation abilities. All the geometric parameters of curve profiles are determined, satisfying the conditions of continuity of tangency requiring only that several specific parameters be given first. The contact lines of the two rotor surfaces and the blowhole area calculation are also presented. Optimization procedure is utilized; three cases of optimization problems are presented in this paper and they show that both the contact-line length and the blowhole area can be reduced when letting the contact-line length be the object function and the blowhole area be the constraint. It provides a useful suggestion for rotor-profile optimization of the screw compressor.

Acknowledgments

This work was supported by National Science Council, Taiwan, Republic of China, under grant number: NSC90-2212-E-009-005.

Nomenclature

C = center distance between two rotors
d = distance from ellipse center to the male rotor center
f_i = equation of meshing of the curve "i" between two rotor profiles
F_i = equation of meshing of the surface "i" between two rotor surfaces
h_1, h_2 = screw parameters of Rotors 1 and 2, respectively.
i = subscript "i"; if $i=e$, that means the ellipse; if $i=c1,c2,c3$, that means the circular arcs $c1,c2,c3$
l = length of the longitudinal axes of the ellipse
m_{21} = ratio of angular velocity
N_1, N_2 = tooth numbers of the male and female rotors, respectively
O_i = center of the curve "i" or the origin of the coordinate system S_i
r_i = radius of the curve "i"
r_{mb1}, r_{ft2} = radii of centrodes for male- and female-rotor profiles, respectively
s = length of latitudinal axes of the ellipse
S_a, S_b = coordinate systems of the male- and female-rotor profiles, respectively (2-D)
S_f = coordinate system of the fixed frame
S_1, S_2 = coordinate systems of the male and female rotors, respectively (3-D)
θ_i = angular parameter of the curve "i"
θ_{m1}, θ_{f1} = initial angles of the tooth on the male and female rotors, respectively
ϕ_1, ϕ_2 = rotation angles or angular displacements of the male and female rotors, respectively
ϕ_1', ϕ_2' = rotation angles of Rotor 1 and Rotor 2 in the meshing process, respectively
ω_1, ω_2 = angular velocities of the male and female rotors, respectively
λ = lead angle of the rotor
ψ_1, ψ_2 = second geometrical parameters of the screw surfaces for Rotors 1 and 2, respectively
$\mathbf{M}_{ij}$ = position vector transformation matrices from coordinate systems "j" to "i"

$\mathbf{N}_i^{(k)}$ = normal vector of the curve ''i'' represented in coordinate system S_k

$\mathbf{r}_i^{(k)}$ = position vector of the curve ''i'' represented in the coordinate system S_k

$\mathbf{r}_{i,conj}^{(k)}$ = position vector of the conjugate curve ''i'' represented in the coordinate system S_k

$\mathbf{r}_{mb1}, \mathbf{r}_{ft2}$ = pitch circles for male- and female-rotor profiles, respectively

$\mathbf{v}_{1,i}^{(k)}, \mathbf{v}_{2,i}^{(k)}$ = velocity of the curve ''i'' of the Rotor 1 and Rotor 2 represented in the coordinate system S_k

$\mathbf{v}_{12,i}^{(k)}$ = relative velocity of the curve ''i'' of the Rotor 1 with respect to Rotor 2 represented in the coordinate system S_k

$\boldsymbol{\omega}_1, \boldsymbol{\omega}_2$ = vectors of angular velocity for the male and female rotors, respectively

$\boldsymbol{\Sigma}_i^{(k)}$ = surface ''i'' represented in coordinate system S_k

$\boldsymbol{\Sigma}_{i,conj}^{(k)}$ = conjugate surface ''i'' represented in coordinate system S_k

References

[1] Mu, A., and Cao, 1993, ''A New Method for the Design of the Twin-Screw Rotors Conjugate Profiles,'' *Proceedings of the 1993 International Compressor Technique Conference at Xi'an*, China, pp. 409–414.

[2] Edstrom, S. E., 1992, ''A Modern Way to Good Screw Rotors,'' *Proceedings of the 1992 International Compressor Engineering Conference at Purdue*, West Lafayette, pp. 421–430.

[3] Tang, Y., and Fleming, J. S., 1993, ''Computer Aided Geometrical Analysis of the Geometrical Characteristics of a Helical Screw Compressor,'' Proceedings of the 1993 International Compressor Technique Conference at Xi'an, China, pp. 400–408.

[4] Bennewitz, C., 1992, ''Software Support for Screw Rotors Design, Manufacture and Quality Control,'' *Proceedings of the 1992 International Compressor Engineering Conference at Purdue*, West Lafayette, pp. 432–438.

[5] Zhang, L., and Hamilton, J. F., 1992, ''Main Geometric Characteristic of the Twin Screw Compressor,'' *Proceedings of the 1992 International Compressor Engineering Conference at Purdue*, West Lafayette, pp. 449–456.

[6] Stosic, N., and Hanjalic, K., 1994, ''Development and Optimization of Screw Engine Rotor Pairs on the Basis of Computer Modeling,'' *Proceedings of the 1994 International Compressor Engineering Conference at Purdue*, West Lafayette, pp. 55–60.

[7] Singh, P. J., and Onuschak, A. D., 1984, ''A Comprehensive, Computerized Method for Twin-Screw Rotor Profile Generation and Analysis,'' *Proceedings of the 1984 International Compressor Engineering Conference at Purdue*, West Lafayette, pp. 519–527.

[8] Stosic, N., and Hanjalic, K., 1996, ''General Method for Screw Compressor Profile Generation,'' *Proceedings of the 1996 International Compressor Engineering Conference at Purdue*, West Lafayette, pp. 157–162.

[9] Stosic, N., and Hanjalic, K., 1997, ''Development and Optimization of Screw Machines With a Simulation Model—Part 1: Profile Generation,'' ASME J. Fluids Eng., **119**, No. 3, pp. 659–663.

[10] Litvin, F. L., and Feng, Pin-Hao, 1997, ''Computerized Design, Generation, and Simulation of Meshing of Rotors of Screw Compressor,'' Mech. Mach. Theory, **32**, No. 2, pp. 137–160.

[11] Lee, H. T., 1990, US Patent 4890992.

[12] Litvin, F. L., 1989, *Theory of Gearing*, NASA RP-1212 (AVSCOM 88-C-035), Washington, D.C..

[13] Litvin, F. L., 1994, *Gear Geometry and Applied Theory*, Prentice Hall, New York.

[14] Singh, P. J., and Bowman J. L., 1990, ''Calculation of Blowhole Area for Screw Compressors,'' *Proceedings of the 1990 International Compressor Engineering Conference at Purdue*, West Lafayette, pp. 938–948.

[15] Tang Y., and Fleming J. S., 1992, ''Obtaining the Optimum Geometrical Parameters of a Refrigeration Helical Screw Compressor,'' *Proceedings of the 1992 International Compressor Engineering Conference at Purdue*, West Lafayette, pp. 221–228.

[16] Zhou Z., 1992, ''Computer Aided Design of a Twin Rotor Screw Refrigerant Compressor,'' *Proceedings of the 1992 International Compressor Engineering Conference at Purdue*, West Lafayette, pp. 457–465.

[17] *Mathematica 3.0*, 1996, Software Produced by Stephen Wolfram Research, Inc..

[18] Yang, T. C., and Tseng, C. H., 1993, ''Integrating and Automating Analysis and Optimization,'' Comput. Struct., **48**, No. 6, pp. 1083–1106.

[19] Tseng, C. H., Liao, W. C., and Yang, T. C., 1993, MOST 1.1 User's Manual. Technical Report No. AODL-93-01, Department of Mechanical Engineering, National Chiao-Tung Univ., Taiwan, R.O.C.

[20] Yoshimura, S., 1990, US Patent 4890991.

[21] Neufville, R., 1990, *Applied System Analysis: Engineering Planning and Technology Management*, McGraw-Hill, New York.